oxidized and semiquinone flavodoxin structures have been solved at 1.9 and 1.8 Å, respectively.[31] The method could be used to compare the monoclinic[32] and orthorhombic[33] crystal forms of yeast phenylalanyl transfer RNA. For proteins having several monomers in the asymmetric unit, such as superoxide dismutase,[34] the volumes of the different monomers could be compared.

**Other Applications.** The method could also be applied to the problem of protein compaction during refinement[27] and to following the volume variation during energy minimizations and molecular dynamics simulations. With modifications, the method could be used to measure empty spaces surrounded by atoms, such as internal cavities or packing defects.[4] Each internal void volume is surrounded by a separate piece of surface. For this case, the analytical partition method would be modified to consider the polyhedron defined by the centers of the atoms surrounding the cavity and to subtract from the volume of this polyhedron the volumes of the internal surface pieces of the cavity. The volumes of ligand-binding pockets on protein surfaces could be measured by developing a way to close off the mouths. The pocket volume would vary somewhat depending on how the capping was done. Interfacial void volumes, for example, those of hemoglobin subunit interfaces,[35] could be measured by defining a polyhedron from the centers of the atoms in the interface and subtracting from its volume the volumes of the surface pieces of these atoms.

**Compatibility with Surface Areas and Graphics.** The analytical partition method fits into a coherent scheme of methods and computer programs for calculating molecular surfaces, measuring their areas and volumes, and displaying them on both vector and raster computer graphics systems.[6,8] The importance of using compatible surface area and volume definitions has been emphasized.[36] The ability to display the analytical partition method graphically (Figures 7 and 8) not only communicates the method but also helps verify its correctness.

(31) Smith, W. W.; Burnett, R. M.; Darling, G. D.; Ludwig, M. L. *J. Mol. Biol.* **1977**, *117*, 195.
(32) Hingerty, B. E.; Brown, R. S.; Jack, A. *J. Mol. Biol.* **1978**, *124*, 523.
(33) Sussman, J. L.; Holbrook, S. R.; Warrant, R. W.; Church, G. M.; Kim, S.-H. *J. Mol. Biol.* **1978**, *123*, 607.
(34) Tainer, J. A.; Getzoff, E. D.; Beem, K. M.; Richardson, J. S.; Richardson, D. C. *J. Mol. Biol.* **1982**, *160*, 181.
(35) Greer, J.; Bush, B. L. *Proc. Natl. Acad. Sci. U.S.A.* **1978**, *75*, 303.
(36) Gates, R. E. *J. Mol. Biol.* **1979**, *127*, 345.

# DNMR and Molecular Mechanics Studies of the Enantiomerization of Long-Chain (1,5)-Naphthalenophanes

**Moon Ho Chang, Brian B. Masek,[1a] and Dennis A. Dougherty*[1b]**

*Contribution No. 7058 from the Division of Chemistry and Chemical Engineering, California Institute of Technology, Pasadena, California 91125.* *Received July 9, 1984*

**Abstract:** The enantiomerizations of several dioxa-(1,5)-naphthalenophanes (**1**: $n$ = 14, 15, 16) have been studied by DNMR spectroscopy, and accurate activation parameters have been obtained. Large, negative entropies of activation are observed when $n$ = 14 or 15. In sharp contrast, $\Delta S^{\ddagger}$ is very nearly zero when $n$ = 16. Molecular mechanics calculations have been applied to these systems in an effort to obtain some insight into the underlying causes of this effect. The results suggest a model in which the polymethylene chains of all three compounds are quite unrestricted and conformationally flexible in the ground state. However, in the enantiomerization transition states when $n$ = 14 or 15, the chain is quite restricted and this leads to the negative $\Delta S^{\ddagger}$. When $n$ = 16, even in the enantiomerization transition state, the chain is relatively unrestricted and $\Delta S^{\ddagger}$ is small.

Macrocyclic organic molecules have been studied intensively in recent years. A major impetus for such work derives from the discovery of a large number of physiologically active substances that contain large rings, including the general classes of the ionophores[2] and the macrolide antibiotics.[3] Additionally, the fast-growing area of synthetic host–guest chemistry is dominated by macrocyclic compounds.[4] All such structures are of interest because they have quite specific binding capabilities, which implies they have well-defined, three-dimensional shapes. However, if one wished to a priori design a structure with a specific shape, a large carbocyclic ring would perhaps be the last starting point one would choose. Such structures are known to be extremely flexible, and to possess a large number of rapidly interconverting conformers.[5] It has been well documented that such "flexibility is the enemy",[6] when designing structures with specific binding properties. In nature, the ionophores and macrolides contain very specific substitution patterns along the chain,[2,3] the reproduction of which continues to be a focal point of modern synthetic organic chemistry. It seems certain that one role of such substituents is to diminish the conformational flexibility of the macrocycles, thereby leading to better defined topographies. In the area of synthetic host–guest chemistry, less subtle approaches to limiting ring flexibility have been adopted, primarily involving the incorporation of structurally rigid units (acetylenes, arenes, . . .) into the ring.

The present work was initiated with the goal of quantifying the effects of specific substituent patterns on macrocycle conformational dynamics. We believe that such information would be

(1) (a) NSF Predoctoral Fellow, 1981–1984. (b) Fellow of the Alfred P. Sloan Foundation, 1983–1985 Camille and Henry Dreyfus Teacher–Scholar, 1984–1989.
(2) Dobler, M. "Ionophores and Their Structures"; Wiley: New York, 1981.
(3) See, for example: Gale, E. F., et al. "The Molecular Basis of Antibiotic Action", 2nd ed.; Wiley: London, 1981.
(4) For a recent overview of the host–guest field, see: "Topics in Current Chemistry"; Vogtle, F., Ed.; Springer Verlag: Berlin, 1981 and 1982; Vol. 98 and 101.
(5) Dale J. *Top. Stereochem.* **1976**, *9*, 199–270. Anet, F. A. L.; Rawdah, T. N. *J. Am. Chem. Soc.* **1978**, *100*, 7166–7171, 7810–7814.
(6) Breslow, R. *Isr. J. Chem.* **1979**, *18*, 187–191.

0002-7863/85/1507-1124$01.50/0 

valuable both in understanding the properties of naturally occurring macrocycles and in designing new synthetic hosts. For such a study to be successful, one must develop a macrocyclic system that meets several specific criteria. First, the system must have an *unambiguously defined*, conformational process involving the large ring. There are a large number of important studies of conformational processes of large rings and polymethylene chains.[5,7] Often, one can quantify a dynamic process in the ring or chain, but the information available does not clearly identify what process is being observed. The second essential criterion is that the rate process involved must be amenable to accurate, *quantitative* evaluation. Finally, the synthesis of the target molecules must be efficient and sufficiently flexible so that one can easily incorporate the various substituent patterns discussed above.

We have chosen as our target molecules the dioxa-(1,5)-naphthalenophanes (**1**), structures which meet all of the above criteria. The cyclophanes **1** are chiral, having at most $C_2$ symmetry. All methylene groups when $n$ is even and all but the central methylene when $n$ is odd consist of a diastereotopic pair of protons. The enantiomers of **1** can interconvert by simply moving the polymethylene chain around to the other face of the naphthalene system, in what Marshall has termed[8] a "jump rope" reaction. This process, and only this process, also interconverts the diastereotopic protons of each methylene group, thereby providing a potential dynamic NMR (DNMR) probe of the enantiomerization. Structures such as **1** thus provide an opportunity for the

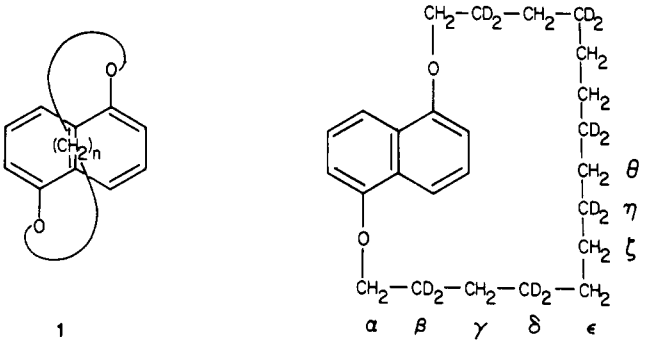


1 C15-D

direct observation of an unambiguously defined conformational process in a macrocyclic compound involving a polymethylene chain. As described below, the synthesis of such structures is quite straightforward, thereby allowing the facile incorporation of a wide range of substituent patterns.

It should be emphasized from the start that such enantiomerization processes are well precedented. The stereochemical phenomenon is identical with that involved in the enantiomerization of trans cycloalkanes, a process that was probed by DNMR almost 20 years ago.[9] There have also been many excellent studies of the dynamic properties of benzenoid cyclophanes and of large-ring cycloalkanes.[5,10] The present structures possess several advantages over these other systems. When compared with *m*- or *p*-cyclophanes (benzenophanes), the (1,5)-naphthalenophanes require only a slight increase in chain length in order to have an equally strain-free ground state. However, the demands on the jump-rope transition state are much more severe, because of the greater "width" of the naphthalene unit relative to a benzene ring. Thus, with the (1,5)-naphthalenophanes one can study much longer chains which are quite flexible and completely strain free in the ground state, but which suffer severe conformational restrictions in the enantiomerization transition state. These systems can thus provide information that is perhaps more relevant to the important properties of macrocycles and long polymethylene chains.

Scheme I

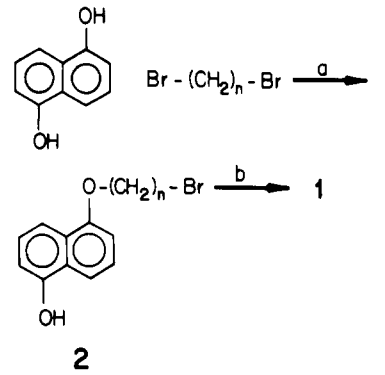


[a] KOH, ethanol. [b] $Me_4NOH$, $Me_2SO$, high dilution.

Scheme II

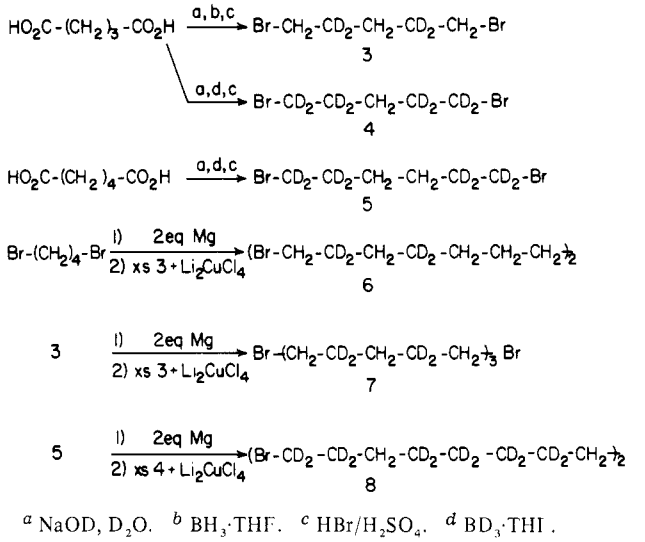


[a] NaOD, $D_2O$. [b] $BH_3$·THF. [c] $HBr/H_2SO_4$. [d] $BD_3$·THF.

In the present work we have employed very high field DNMR to obtain highly accurate activation parameters for the enantiomerizations of molecules such as **1**. We have, thus far, studied **1** with $n$ = 14, 15, and 16—structures we shall refer to as C14, C15, and C16. A detailed understanding of the dynamics of these unsubstituted chains is necessary before we can address the issue of substituent effects. Additionally, polymethylene chains are of interest in their own right, because of the important role such structural units play in phospholipid bilayers, micelles, vesicles, and related structures. Our results have uncovered substantial conformational restrictions in the enantiomerization transition states, as manifested by very large, negative entropies of activation. Our studies also reveal the dangers of extrapolating activation parameters among even very closely related structures. We have also applied the molecular mechanics (MM) method[11] to such structures, in the hope of obtaining more detailed information on both the static and dynamic properties of these systems.

## Synthesis

As discussed above, we intend to study a wide variety of long chains in order to probe the influence of chain length, substituents, and solvents on the conformational process. The synthesis of the cyclophanes must therefore be simple, efficient, and general enough to allow preparation of a wide variety of structures. For this reason, we chose the dioxa-(1,5)-naphthalenophanes **1** as our target

(7) For a recent review, see: Winnik, M. A. *Chem. Rev.* **1981**, *81*, 491–524.
(8) Marshall, J. A. *Acc. Chem. Res.* **1980**, *13*, 213–218.
(9) Binsch, G.; Roberts, J. D. *J. Am. Chem. Soc.* **1965**, *87*, 5157–5162.
(10) For studies on systems related to **1**, see: Whitesides, G. M.; Pawson, B. A.; Cope, A. C. *J. Am. Chem. Soc.* **1968**, *90*, 639–644. Förster, H.; Vögtle, F. *Angew. Chem., Int. Ed. Engl.* **1977**, *16*, 429–441. Brown, H. S.; Muenchausen, C. P.; Sonsa, L. R. *J. Org. Chem.* **1980**, *45*, 1682–1686. Whitlock, B. J.; Whitlock, H. W. *J. Am. Chem. Soc.* **1983**, *105*, 838–844.

(11) Burkert, U.; Allinger, N. L. "Molecular Mechanics"; American Chemical Society: Washington, D.C., 1982.

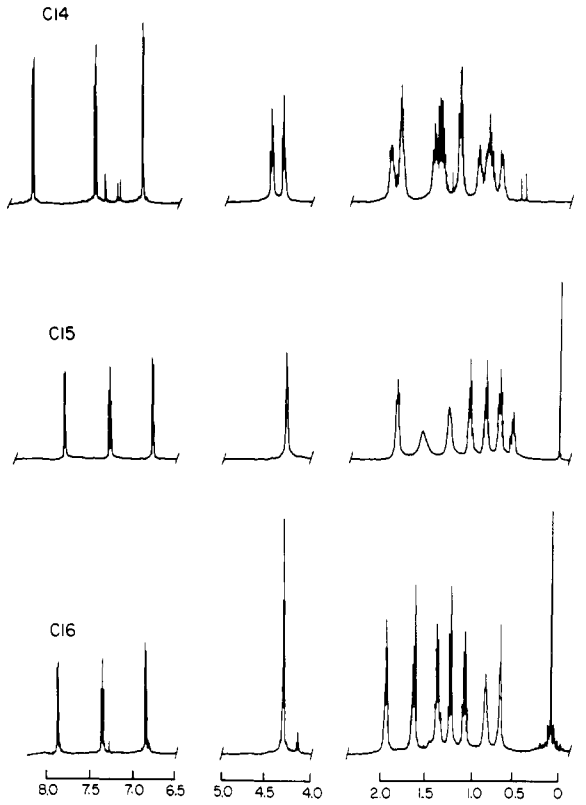


**Figure 1.** 500-MHz $^1H$ NMR spectra in $CDCl_3$ (C16), $CCl_4$ (C15), or *o*-dichlorobenzene-$d_4$ (C14) at ambient probe temperatures. Chemical shifts are in ppm relative to $Me_4Si$. Signals at ca. 1.6 and 1.3 ppm for C15 are broadened at this temperature because of the exchange process.

molecules, rather than pure hydrocarbons. Using procedures developed by Mandolini,[12] such cyclophanes can be prepared efficiently in two steps, starting from the readily available 1,5-dihydroxynaphthalene (Scheme I).

A wide variety of long-chain, $\alpha,\omega$-dibromides are readily available, thus allowing the synthesis of many cyclophanes. More importantly, substituted derivatives of such structures can be prepared easily. As described below, preliminary studies revealed that the third ($\gamma$) $CH_2$ from the oxygen in the chain was the most useful DNMR probe in such molecules. As such, we wished to fully deuterate the second ($\beta$) and fourth ($\delta$) $CH_2$'s, so as to isolate the $\gamma$ signal. This could be done easily as shown in Scheme II. Base-catalyzed $^2H$ exchange in glutaric acid is straightforward, and this unit provides the isolated $\gamma$ $CH_2$, ultimately as dibromide **3** or **4**. A deuterated six-carbon unit can be similarly prepared (**5**). Then, through a simple coupling of Grignard reagents, highly deuterated, $\alpha,\omega$-dibromides with 14, 15, and 16 carbons can be prepared easily (Scheme II). For example, from dibromide **7** (Scheme II), C15-D results, which contains $^2H$ at the $\beta$, $\delta$, and $\eta$ positions (see drawing for labeling). The generality of the coupling reaction allows the synthesis of long chains with isolated $\gamma$ protons and almost any substituents in the center of the chain, by simply coupling the readily available **3** with an appropriate dibromide.

## DNMR Results

**Ambient Temperature, Static NMR.** Figure 1 shows the 500-MHz $^1H$ NMR of C14, C15, and C16 at ambient probe temperatures. Although such structures may be asymmetric in the ground state, one can expect that conformational interconversions that are rapid on the NMR timescale will occur so that the structures have either real, or time-averaged $C_2$ symmetry. If the jump-rope reaction is slow (on the NMR timescale) at ambient temperatures, one would expect 14, 15, and 16 aliphatic signals for C14, C15, and C16, respectively, due to the diastereotopic methylenes. If the jump-rope reaction is fast, each $CH_2$ group produces only one signal and one expects seven, eight, and eight aliphatic signals for C14, C15, and C16, after consideration of the $C_2$ symmetry.

Inspection of Figure 1 shows clearly that the jump-rope reaction is rapid for C15 and C16 at ambient temperatures. Remarkably, one sees eight, base-line-resolved signals for each structure. This remarkable separation of the signals of eight $CH_2$ groups in a chain results from three effects: the use of high-field NMR, the highly anisotropic environment provided by the naphthalene, and the normal chemical shift effects of the ether oxygen. For both C15 and C16, all of the aliphatic resonances have been unambiguously assigned. If one labels the $CH_2$ next to oxygen as $\alpha$, and then continues to $\beta$, $\gamma$, etc., the $\alpha$ signal can immediately be assigned by its chemical shift (ca. 4.2 ppm). The middle ($\theta$) $CH_2$ of C15 is identified as the most upfield signal by its intensity, which is half that of any other $CH_2$ because it lies on the twofold symmetry axis. Straightforward decoupling experiments and $^2H$ labeling studies (see below) allow complete assignments for both spectra. In each case, the sequence of $^1H$ NMR signals from low field to high precisely parallels the progression of methylenes along the chain, starting with the $-OCH_2$ group. The $CH_2$'s toward the middle of the chains are significantly shielded relative to normal methylenes. The fact that the most shielded methylene is the middle ($\theta$) group could be an indication that the most strongly shielding region of a naphthalene system lies directly above the center of inversion of the ring system.

The situation is clearly different for C14 (Figure 1). The $\alpha$ protons are an AB pattern with additional coupling, and the rest of the aliphatic region is much more complex. The jump-rope reaction is slow at ambient temperatures in C14, and although one sees more than 7 signals, the expected 14 aliphatic signals are not completely resolved. By analogy to C15 and C16 and by $^2H$ labeling studies (see below), we believe that the chemical shift assignments for C14 follow the same pattern as for C15 and C16. Note that the aromatic region is essentially identical for all three structures (Figure 1). This is because the aromatic signals are unaffected by the jump-rope reaction, a fact that is also apparent in the DNMR studies described below.

**C14—Complete Line Shape.** Based on our studies with C15 and C16 (see below) and on preliminary work with C14, it was decided that the $\gamma$ $CH_2$ would be the best candidate for DNMR studies. This is because for all three structures the chemical shift separation ($\Delta\nu$) is greater for the AB pattern of the $\gamma$ than for any other methylene. The greater $\Delta\nu$ is, the greater the temperature range over which coalescence occurs and thus the greater the temperature range over which reliable reaction rates can be obtained. This leads to more reliable activation parameters.[13] We therefore prepared C14-D by inserting dibromide **6** into Scheme I. In this molecule the $\beta$ and $\delta$ positions are fully deuterated.

Preliminary DNMR studies on C14-D at 500 MHz revealed that we could not safely attain temperatures high enough to achieve satisfactory coalescence. This is one case for which operating at a very high spectrometer field is a disadvantage. We therefore undertook a DNMR study of the $\gamma$ $CH_2$ of C14-D at 200 MHz. The relevant spectra are shown in Figure 2, along with simulations obtained by the complete line-shape (CLS) method.[14] The value of $\Delta\nu$ was dependent upon temperature, and in the fast exchange region the value of $\Delta\nu$ used in the CLS was obtained by linear extrapolation of values obtained in the very slow exchange region. The value used for the effective $T_2$ in the CLS studies ($T_{2eff}$) was obtained by using the high-field aromatic doublet ($\delta$ 6.95) as an internal standard. The relevant rates are collected

(12) (a) Dalla Cort, A.; Mandolini, L.; Masci, B. *J. Org. Chem.* **1980**, *45*, 3923–3925. Mandolini, L.; Masci, B.; Roelens, S. *Ibid.* **1977**, *42*, 3733–3736. (b) We have recently discovered that the naphthalenophanes can be efficiently prepared in one step by coupling the dibromide and the diol in DMF using $Cs_2CO_3$ as the base. (c) Structure **1** with $n = 10$ was reported previously: Luttringhaus, A. *Justus Liebigs Ann. Chem.* **1937**, *528*, 181–210.

(13) Binsch, G.; Kessler, H. *Angew. Chem., Int. Ed. Engl.* **1980**, *19*, 411–428.

(14) For an excellent overview of the DNMR method, see: Sandström, J. "Dynamic NMR Spectroscopy"; Academic Press, New York, 1982.

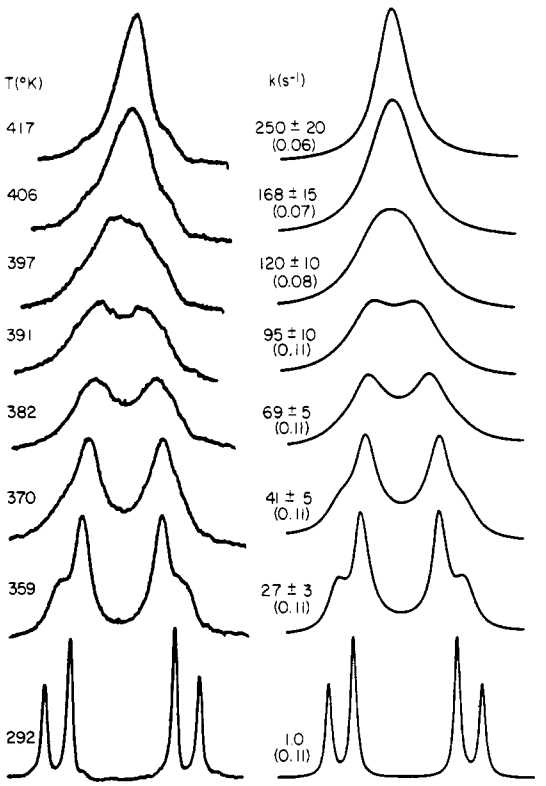


**Figure 2.** 200-MHz, variable-temperature, $^1$H NMR spectra of the $\gamma$ protons of C14-D (nitrobenzene-$d_5$). At 292 K, the AB pattern corresponds to: $\Delta\nu$ = 69 Hz, $J$ = 13.6 Hz. $T_{2\text{eff}}$ values are listed below the rate constants.

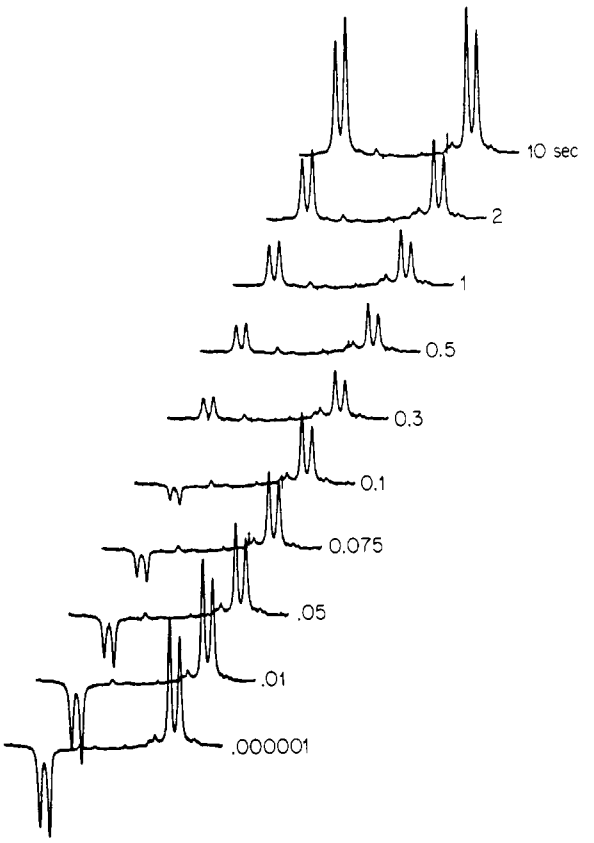


**Figure 3.** C14-D, SST experiment at 318 K (500 MHz, *o*-dichlorobenzene-$d_4$). Numbers beside the AB patterns correspond to the time delay in seconds between inversion and acquisition.

**Table I.** Enantiomerization Rates

| | | $T$ (K)[a] | $k$ ($s^{-1}$) |
|---|---|---|---|
| C14 | 200 MHz CLS[b] | 359 | 27 ± 3 |
| | | 370 | 41 ± 5 |
| | | 382 | 69 ± 5 |
| | | 391 | 95 ± 10 |
| | | 397 | 120 ± 10 |
| | | 406 | 168 ± 15 |
| | | 417 | 250 ± 20 |
| | 500 MHz SST[c] | 303 | 1.4 ± 0.1 |
| | | 313 | 2.9 ± 0.2 |
| | | 318 | 4.1 ± 0.3 |
| | | 324 | 5.3 ± 0.3 |
| | | 329 | 6.5 ± 0.4 |
| C15 | 500 MHz CLS[d] | 246 | 52 ± 4 |
| | | 253 | 82 ± 4 |
| | | 260 | 126 ± 4 |
| | | 266 | 182 ± 6 |
| | | 272 | 256 ± 6 |
| | | 279 | 357 ± 8 |
| | | 288 | 590 ± 20 |
| | 90 MHz CLS[d] | 238 | 29 ± 3 |
| | | 241 | 35 ± 3 |
| | | 244 | 44 ± 4 |
| | | 250 | 68 ± 6 |
| | | 252 | 73 ± 7 |
| | | 255 | 94 ± 9 |
| | | 261 | 130 ± 10 |
| C16 | 500 MHz CLS[e] | 186 | 30 ± 3 |
| | | 194 | 90 ± 5 |
| | | 201 | 190 ± 10 |
| | | 210 | 555 ± 50 |
| | | 219 | 1460 ± 150 |
| | | 227 | 3000 ± 200 |
| | | 234 | 4900 ± 300 |

[a] ±1 K. [b] In nitrobenzene-$d_5$. [c] In *o*-dichlorobenzene-$d_4$. [d] In $CD_2Cl_2$. [e] In $CF_2Cl_2/CD_2Cl_2$, 19:1.

in Table I, and derived activation parameters and related data are listed in Table II. A complete discussion of the accuracy of these results will be presented below, but we note at this point that a quite satisfactory correlation is obtained (Table II).

**C14—Saturation Spin Transfer.** Because our goal is to obtain highly reliable activation parameters for the jump-rope reaction, and because of the well-known hazards of extracting such data from CLS analysis, we desired a second check on the CLS data. This was especially so because of our inability to use very high field NMR for C14 and because of the intriguing observation of a very large, negative value for $\Delta S^{\ddagger}$ (Table II). We therefore applied the saturation spin transfer (SST or magnetization transfer) technique to C14-D.[15]

In order to apply the SST method to C14, one must deliver a selective 180° pulse to one-half of the AB pattern (Figure 2) of the $\gamma$ proton. Such selectivity is difficult to achieve when the signals are too close, and so the 500-MHz NMR spectrometer was used to obtain maximum signal separation. The selective pulse was delivered by a DANTE pulse sequence,[16] and the inversion recovery was monitored in the usual way. A typical experiment is shown in Figure 3. Table I lists the rate constants obtained in this manner. The useful feature of the SST method is that it measures rates that are roughly comparable to $1/T_1$. This is in contrast to the standard DNMR (coalescence) approach, which measures rates that are roughly comparable to the chemical shift separation. The two methods therefore work in different rate (and thus temperature) regimes, and together they can cover a very broad kinetic range.

The results from the SST method are in excellent agreement with those from CLS. This can be seen in Table II, which includes activation parameters for the SST data and for the combined CLS and SST data, and from Figure 4, which shows the Eyring plot for the combined data.[17] By combining the two methods, reliable rates are obtained over a 114° temperature range, which greatly

(15) See, for example: Dahlquist, F. W.; Longmuir, K. J.; DuVernet, R. B. *J. Magn. Reson.* **1975**, *17*, 406–410.
(16) Morris, G. A.; Freeman, R. *J. Magn. Reson.* **1978**, *29*, 433–462.
(17) For an early example of the combined use of CLS and magnetization transfer data, see: Anet, F. A. L.; Bourn, A. J. R. *J. Am. Chem. Soc.* **1967**, *89*, 760–768.

**Table II.** Activation Parameters for Enantiomerization Reactions

| | $\Delta H^{\ddagger}$ [a] | $\Delta S^{\ddagger}$ [b] | $\Delta G^{\ddagger}_{298}$ [a] | $\rho$ [c] | $\sigma\Delta H^{\ddagger}$ [d] | $\sigma\Delta S^{\ddagger}$ [d] | no. of pts [e] | $\Delta T$ [f] |
|---|---|---|---|---|---|---|---|---|
| | | | | C14 | | | | |
| 200 MHz CLS | 10.72 | −22.6 | 17.44 | 0.9996 | 0.14 | 0.35 | 7 | 58 |
| 500 MHz SST | 11.03 | −21.4 | 17.40 | 0.9927 | 0.77 | 2.43 | 5 | 26 |
| CLS + SST | 10.39 | −23.4 | 17.36 | 0.9995 | 0.10 | 0.29 | 12 | 114 |
| | | | | C15 | | | | |
| 500 MHz CLS | 7.56 | −19.6 | 13.39 | 0.9997 | 0.09 | 0.32 | 7 | 42 |
| 90 MHz CLS | 7.68 | −19.2 | 13.39 | 0.9989 | 0.16 | 0.64 | 7 | 23 |
| 90 ± 500 MHz CLS | 7.65 | −19.3 | 13.38 | 0.9997 | 0.06 | 0.21 | 14 | 50 |
| | | | | C16 | | | | |
| 500 MHz CLS | 8.83 | −3.3 | 9.81 | .9994 | 0.14 | 0.65 | 7 | 48 |

[a] kcal/mol. [b] cal/mol·K. [c] Correlation coefficient. [d] Standard deviation. [e] Number of data points. [f] Temperature range.

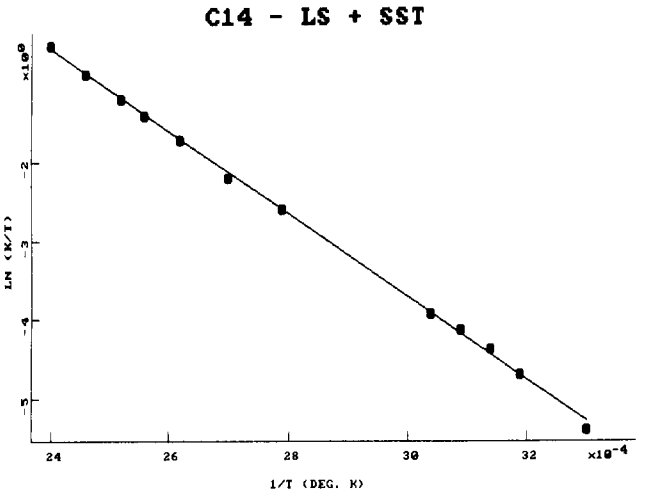


**Figure 4.** Eyring plot for C14-D, combined CLS and SST data.

increases the confidence one has in the derived activation parameters. It should be noted that, for technical reasons, the SST and CLS studies were done in different solvents (*o*-dichlorobenzene and nitrobenzene, respectively). The fact that all the data fall on the same Eyring line (Figure 4) indicates that, as expected, there is no significant solvent effect on the jump-rope reaction.

**C15.** Standard kinetic analyses by the CLS method at 500 MHz proceeded especially smoothly for C15 (Figure 5, Table I).[18] Again the deuterated molecule C15-D (prepared from dibromide **7**) was used so that the AB pattern of the $\gamma$ protons was fully isolated. The CLS study of C15-D had two significant advantages over those of C14 and C16. First, there was no evidence for a temperature-dependent $\Delta\nu$ for the $\gamma$ protons, although such an effect was clearly evident for the $\alpha$ protons. Second, the deuteration pattern also isolated the $\theta$ protons, which are symmetry equivalent regardless of the jump rope rate because the $\theta$ carbon lies on the molecular $C_2$ axis. The $\theta$ protons in C15-D therefore remain a sharp singlet throughout the DNMR temperature range. As such, they provide an excellent internal probe for determining the $T_{2eff}$ value to be used in the CLS study, because they are on the chain that is undergoing the conformational process being studied. The $T_{2eff}$ values used in the CLS for the $\gamma$ protons were thus based on the width of the $\theta$ signal, corrected by the ratio of widths of the $\gamma$ and $\theta$ signals at the low-temperature limit. While we felt that the $\theta$ protons were the ideal probe for measuring $T_{2eff}$, we did note that use of either the solvent signal ($CHDCl_2$) or the aromatic resonances as references gave comparable $T_{2eff}$ values over the temperature range studied at 500 MHz. This supports our use of these signals as references for C14 and C16.

Both of the above factors increase the reliability of the CLS study of C15-D considerably. As shown in Table II, an excellent correlation was obtained. Also shown in Tables I and II are data obtained from a study of C15-D at 90 MHz. Because of the smaller chemical shift separation at 90 MHz, the temperature range amenable to study is rather small, and the Eyring fit of the CLS data is less satisfactory. However, the agreement between the results from studies on two different spectrometers is excellent (Table II).

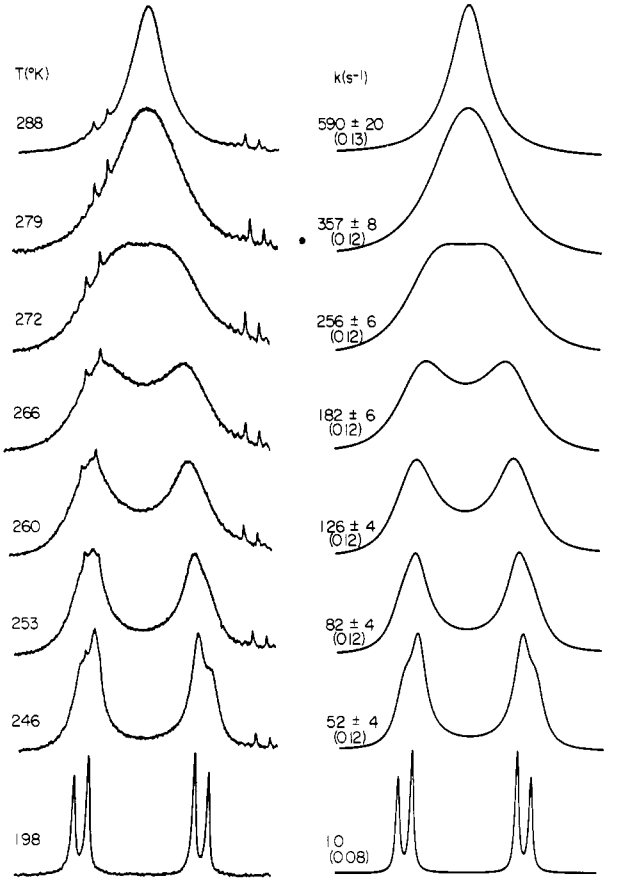


**Figure 5.** 500-MHz, variable-temperature, $^1H$ NMR spectra of the $\gamma$ protons of C15-D ($CD_2Cl_2$). At 198 K, the AB pattern corresponds to: $\Delta\nu$ = 116.7 Hz, $J$ = 13.7 Hz. $T_{2eff}$ values are listed below the rate constants.

**C16.** The DNMR study for C16 proceeded smoothly at 500 MHz, and the results along with the CLS data are given in Figure 6. Again the $\gamma$ protons were studied, and the temperature dependence of $\Delta\nu$ and $T_{2eff}$ were treated as for C14. Because $\Delta\nu$ for the $\gamma$ protons was quite large (362 Hz at the low-temperature limit), extensive $^2H$ labeling was necessary to avoid overlap of signals and dibromide **8** was used to prepare C16-D. The derived rates and activation parameters are given in Table I and II. Note that a very much larger range of rates could be measured for C16 than for C14 or C15 by CLS. In fact, the CLS study for C16 spanned a range of rates quite comparable to that of the combined CLS plus SST data for C14. This was possible because of the very large $\Delta\nu$ and the relatively greater sensitivity of the rate to temperature for C16.

(18) The primary results for C15 have been reported previously: Chang, M. H.; Dougherty, D. A. *J. Am. Chem. Soc.* **1983**, *105*, 4102–4103.

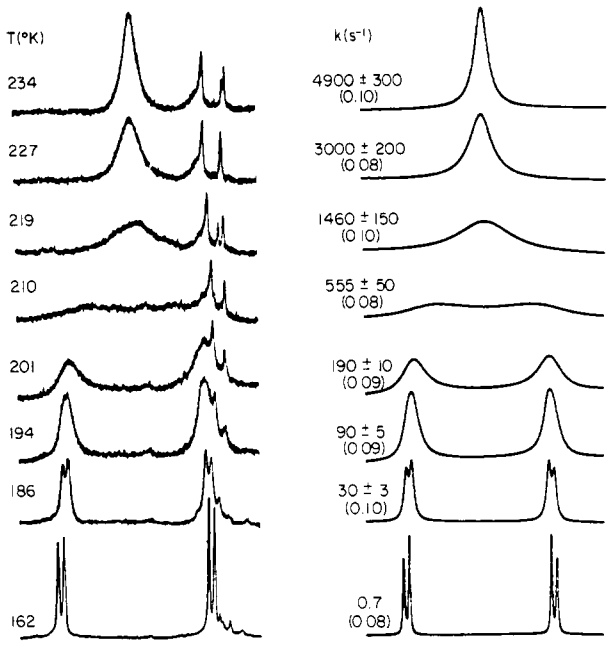


**Figure 6.** 500-MHz, variable-temperature, $^1$H NMR spectra of the $\gamma$ protons of C16-D ($CF_2Cl_2/CD_2Cl_2$, 19:1). At 162 K, the AB pattern corresponds to: $\Delta\nu$ = 362 Hz, $J$ = 13.6 Hz. $T_{2eff}$ values are listed below the rate constants.

The $\theta$ protons of C16-D were the only other observable protons, and their variable-temperature behavior was remarkable. At 288 K, the $\theta$ protons of C16-D are a sharp singlet at 0.62 ppm. At the low-temperature limit, the $\theta$ protons should exhibit an AA'BB' pattern, and, on cooling to 162 K two broad signals are observed. These signals are separated by 434 Hz and are located at $\delta$ +0.55 and −0.32 ppm, giving a midpoint of +0.115 ppm. Thus, a substantial upfield shift of the $\theta$ protons occurs on cooling, such that one of the signals is in a very highly shielded environment. While $\Delta\nu$ for the $\gamma$ protons in C14 and C16 is temperature dependent, the midpoint of the $\gamma$ signal does not change for any of the compounds studied. Perhaps at lower temperatures, the time-averaged structure of C16 is such that the middle of the chain is more collapsed toward the naphthalene, thus providing the greater overall shielding of the $\theta$ proton.

### Error Limits

The DNMR method has long been recognized as a valuable tool for obtaining rate data.[13,14] There are, however, many hazards in using such data to obtain reliable activation parameters from the CLS method.[13] The difficulty arises because several factors other than the rate process of interest can affect line shapes. These include changes in $T_{2eff}$ due to field inhomogeneity at different temperatures or to changes in solvent viscosity which lead to altered molecular tumbling rates and thus altered relaxation times. Another complicating factor is temperature-dependent chemical shifts. Consideration of these effects is especially important in the early and late regions of the coalescence, where line broadening due to exchange is relatively small.

We felt from the outset that through a combination of high-field NMR and the highly anisotropic environment provided by the naphthalene ring we could minimize such problems. These two factors combine to produce quite large $\Delta\nu$ values for the $\gamma$ protons of the three structures studied. Because of the large value of $\Delta\nu$, the coalescence process occurs over a very broad temperature range. We can therefore ignore the early and late regions of the coalescence, and consider only signals that are very substantially broadened (line widths at least six times greater than those at the low-temperature limit).[13] This greatly minimizes the contributions of factors other than chemical exchange to the broadening. One can only do this, and still obtain rates over a large enough temperature range for accurate Eyring analysis, when $\Delta\nu$ is quite large. Another favorable factor for the present system is the presence of an internal reference signal in each molecule (the aromatic protons for all three structures and additionally the $\theta$ protons for C15-D) that allows reliable $T_{2eff}$ values to be obtained. The virtues of this approach have been discussed previously.[19]

**Table III.** Activation Parameters with Estimated Error Limits[a]

| structure | $\Delta G^\ddagger$ | $\Delta H^\ddagger$ | $\Delta S^\ddagger$ |
|---|---|---|---|
| C14 | 17.4 ± 0.2 | 10.4 ± 0.5 | −23 ± 2 |
| C15 | 13.4 ± 0.2 | 7.6 ± 0.7 | −20 ± 2 |
| C16 | 9.8 ± 0.2 | 8.8 ± 0.4 | −3 ± 2 |

[a] Units are kcal/mol and cal/mol·K.

The activation parameters and associated data were obtained using an iterative procedure that considers the errors in both the rates and the temperatures.[20] The errors in the rates were estimated by considering the range of rates that gave acceptable fits to the experimental data. Temperatures were considered accurate to ±1 K. The temperature controllers used maintained the temperature within a much smaller range than this.

As shown in Table II, quite excellent correlations were obtained for all of the high-field LS studies. There has been much criticism of the use of correlation coefficients as criteria for goodness-of-fit to a straight line,[21] but the values in Table II certainly indicate good correlations.

The least satisfactory data come from the SST method as applied to C14-D. It shows a significantly worse correlation coefficient, and much worse standard deviations in $\Delta H^\ddagger$ and $\Delta S^\ddagger$ than the other methods. When coupled with the relatively narrow temperature range amenable to study by the technique, we conclude that the SST approach alone cannot provide reliable activation parameters for systems such as the present one without additional data. We hasten to add that the present system is not an ideal one for the SST method. The closeness of the two exchanging signals makes it difficult to deliver a completely selective 180° pulse. Additionally, the fact that we are observing doublets, rather than singlets, makes integration less reliable. For well-separated, intense singlets the method should be more accurate.

It is generally agreed that, given the possibilities for systematic error in DNMR studies, the standard deviations in $\Delta H^\ddagger$ and $\Delta S^\ddagger$ derived from an Eyring plot are inadequate measures of probable error.[13,14] We have adopted the approach suggested by Sandström.[19] This method assumes maximal errors of 10% in rate constants, and 1.0 K in temperatures to determine a maximal error in $\Delta G^\ddagger$, and assumes the error in all points equals the maximal error in deriving errors for $\Delta H^\ddagger$ and $\Delta S^\ddagger$. Using this approach, we arrive at the best estimates for activation parameters listed in Table III. The error limits so derived represent at least three standard deviations — and generally much more — and we feel they are quite realistic.

The fundamental conclusion of the DNMR studies can thus be stated with some confidence. The enantiomerizations of both C14 and C15 exhibit very large, negative entropies of activation, when compared with typical, nonpolar unimolecular processes. In sharp contrast, $\Delta S^\ddagger$ for C16 is quite close to zero, a typical value for an ordinary conformational process.[22]

### Molecular Mechanics Calculations

In conjunction with our DNMR studies, we have also applied the MM method[11] to the naphthalenophanes. We wished to address two issues with such studies. First, we hoped to obtain some more precise information on the static and dynamic properties of **1** in order to perhaps rationalize the remarkable results of Table III. Second, we wished to evaluate the applicability of the MM approach to molecules such as **1**. While it is true that the method has been applied to molecules that are significantly

(19) Berg, U.; Karlsson, S.; Sandström, J. *Org. Magn. Reson.* **1977**, *10*, 117–121.
(20) Irvin, J. A.; Quickenden, T. I. *J. Chem. Educ.* **1983**, *60*, 711–712.
(21) See, for example: Davis, W. H., Jr.; Pryor, W. A. *J. Chem. Educ.* **1976**, *53*, 285–287. Hancock, C. K. *Ibid.* **1965**, *42*, 608–609.
(22) In priciple, there must be a kinetic isotope effect on the isomerization, but we feel that such an effect will be very small and will not affect the fundamental conclusions of this study.

larger than, e.g., C16, generally such structures have been relatively rigid, polycyclic molecules. As will be demonstrated below, the extensive flexibility of structures such as **1** make them much more challenging targets for MM calculations.

We have used two different empirical force fields for the MM calculations. The first is the standard, full MM calculation using Allinger's MM2 force field[11,23] and the BIGSTRN3 program.[24] The second was a simplified version of this approach which does not explicitly treat the hydrogen atoms of a given structure. Instead, "extended atoms" are used for calculating van der Waals interactions. For example, a $CH_2$ group is treated as a spherical atom offset from the position of the carbon in the direction of idealized hydrogens. Such an approach can greatly diminish the amount of computing time necessary for energy evaluations and geometry optimizations, and is often used in MM studies of larger molecules such as proteins. The particular parameters used were those of the NOH (no-hydrogen) field developed by Still and implemented in the program MODEL.[25] In general, this second approach is expected to be less accurate than a full MM calculation, but it is extremely useful in preliminary evaluations of complicated systems.

Generally, MM calculations are used to provide some insight into the origins of the enthalpic component of conformational barriers. In principle, one could use the standard angle driving technique to produce, in the present case, an enantiomerization reaction path. This would lead directly to a value for $\Delta H^{\ddagger}$. However, using MM2, all attempts at so doing were unsuccessful. For example, the $\alpha$ angle in C12 (see below for structural details) can be driven in increments through a full 360° without forcing the chain around to the other face of the naphthalene. This is because the chain is so flexible in the ground state (see below) that it can continuously readjust as it is driven, and it is never forced to jump rope. Only by simultaneously driving several angles could one hope to achieve a computational jump rope. However, this is tantamount to enforcing a preconceived mechanism upon the reaction, and so we have resisted this approach.

Some valuable insights, though, can be obtained from Figure 7, which shows the torsional profiles for anisole and 1-methoxynaphthalene as calculated using both the NOH and MM2 fields. The undefined parameters for MM2[26] were chosen so as to reproduce both the experimental barrier for rotation in anisole and the existing structural data for anisole and related compounds.[27] The standard NOH parameters were used, and as can be seen they are in fair agreement with MM2. The more accurate MM2 procedure predicts an 8-kcal/mol barrier for rotation of a methoxy group past the peri hydrogen (H8) of naphthalene. This is quite similar to the $\Delta H^{\ddagger}$ values seen for C14–C16. In an idealized enantiomerization pathway, one end of the chain would go past the peri position and the other past the 2 position. This suggests that a major contributor to $\Delta H^{\ddagger}$ is this peri interaction, with relatively little steric strain due to interactions involving the remainder of the chain wrapping around the naphthalene.

Our major goal in applying MM to the present problem was to gain some insight into the remarkable $\Delta S^{\ddagger}$ values of Table III.

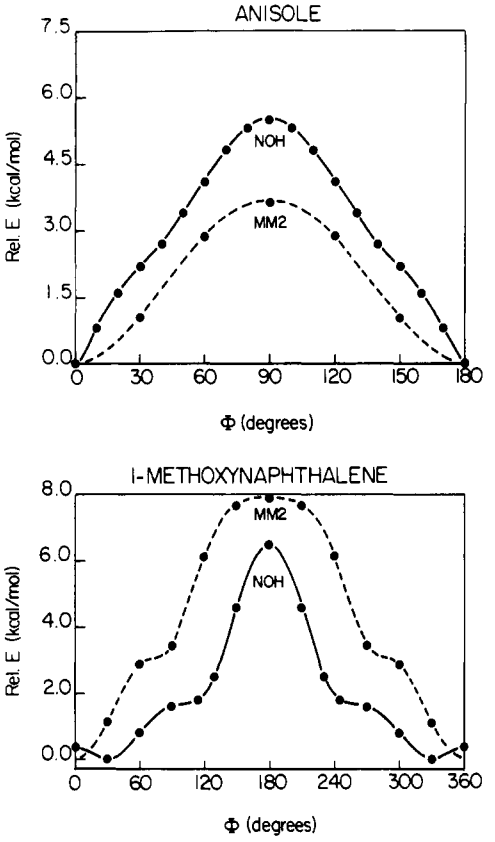


**Figure 7.** Calculated torsional profiles for anisole and 1-methoxynaphthalene using the MM2 and NOH force fields. The dihedral angle $\Phi$ is the C2–C1–O–$CH_3$ angle for both structures.

Inspection of molecular models and preliminary calculations using standard approaches for generating input structures indicated that a very large number of structures with relatively low energies were possible for **1**. This was true even for relatively short chains (e.g., C12). As such, some unambiguous and complete method for generating all plausible input structures for the MM calculations was necessary.

To address this problem, a computer program was written to generate all possible chains reaching from one oxygen in **1** to the other.[28] The naphthalene system and the two oxygens were fixed at standard geometries.[29] Starting at one oxygen and looping toward the other, the chain was built up using standard bonding parameters. The dihedral angles are labeled in a manner analogous to our labeling of $CH_2$ groups along the chain. The first angle, $\alpha$, is the $C(2)_{aryl}$–$C(1)_{aryl}$–O–$CH_2$ angle, the $\beta$ angle is $C_{aryl}$–O–$CH_2$–$CH_2$, etc. In this manner, the $\alpha$ angle positions the $\alpha$ carbon, the $\beta$ angle positions the $\beta$ carbon, etc. Each dihedral angle along the chain was allowed to be either gauche (+), gauche (−), or anti (C–C–C–C angles of 60, −60, or 180°, respectively). The only exception was $\alpha$ which was allowed to assume any value between −135 and +135° in 45° increments. To represent the naphthalene system, an ellipsoidal region into which the chain could not enter was used. This prevented the generation of structures for which the chain passed "through" the naphthalene.

Any chain that terminated within a specified distance of the terminal oxygen (the closure criterion) was retained. All such structures were then submitted to a closure "optimization" procedure. The goal of this process was to make the C–O bond length and the $CH_2$–$CH_2$–O and $CH_2$–O–$C_{aryl}$ bond angles of the closure conform to standard bonding parameters. This was accomplished by allowing the dihedral angles along the chain to deviate slightly from the standard values and retaining any deviation that led to

(23) Allinger, N. L. *J. Am. Chem. Soc.* **1977**, *99*, 8127–8134. Allinger, N. L.; Chang, S. H. M.; Glaser, D. H.; Hönig, H. *Isr. J. Chem.* **1980**, *20*, 51–56.

(24) Bürgi, H. B.; Hounshell, W. D.; Nachbar, Jr., R. B.; Mislow, K. *J. Am. Chem. Soc.* **1983**, *105*, 1427–1438.

(25) Still, W. C., unpublished results.

(26) Bond stretching: 4–12; $K$ = 771.63 kcal/mol·$A^2$. Angle bending: 12–12–4, $K$ = 79.21 kcal/mol·$rad^2$; 12–4–2, $K$ = 110.85 kcal/mol·$rad^2$; 12–4–5, $K$ = 50.39 kcal/mol·$rad^2$. Torsions (kcal/mol):

| angle | $V_0$ | $V_1$ | $V_2$ | $V_3$ |
|---|---|---|---|---|
| 12-12-12-4 | 14.736 | −0.270 | −15.0 | 0.0 |
| 4-12-12-1 | 15.0 | 0.0 | 0.0 | −15.0 |
| 12-12- 4-5 | 0.0 | 0.0 | 0.0 | 0.0 |
| 12- 4- 2-2 | 0.347 | 0.400 | −0.520 | 0.467 |
| 12- 4- 2-1 | 0.530 | 0.0 | 0.0 | 0.530 |

Dipole, 12–4; 0.44 D.—where 1 = H, 2 = C, 4 = O, 5 = lone pair, 12 = $C_{aryl}$.

(27) Anderson, G. M.; Kollman, P. A.; Domelsmith, L. N.; Houk, K. N. *J. Am. Chem. Soc.* **1979**, *101*, 2344–2352.

(28) A similar approach is used in the program RINGMAKER: Still, W. C.; Galykner, I. *Tetrahedron* **1981**, *37*, 3981–3996.

(29) Cruickshank, D. W. J.; Sparks, R. A. *Proc. R. Soc. London* **1960**, *258*, 270–285.

**Table IV.** Distribution of the Dihedral Angles in the 778 Minima for C12

| angle | gauche (−) | gauche (+) | anti |
|---|---|---|---|
| $\beta$ | 731 | 673 | 152 |
| $\gamma$ | 544 | 437 | 575 |
| $\delta$ | 394 | 400 | 762 |
| $\epsilon$ | 516 | 493 | 547 |
| $\zeta$ | 461 | 430 | 665 |
| $\eta$ | 374 | 390 | 792 |
| $\theta$ | 261 | 250 | 267 |

a decrease in the energetics of the ring closure. These energetics were evaluated using the standard MM terms for the three parameters described above. After this procedure, all generated structures had standard bond lengths and valence angles along the entire chain. Finally, each structure generated in this manner was subjected to an initial energy evaluation using NOH.

The number of unique structures generated in the above manner was surprisingly large. Our initial studies emphasized C12 as the smallest structure that, according to models, still seemed reasonably flexible in the ground state. For example, with the initial closure criterion at 3.5 Å, we generated all viable C12 structures and then "optimized" the ring closure. The steric energy of each structure was then evaluated using the NOH field, and only structures with steric energies less than 200 kcal/mol were retained. The energy of the most stable structure, $E_0$, was 55 kcal/mol. Using this approach, 1906 unique, C12 input guesses were obtained. In this context, unique implies having a different value of the conformational descriptor assigned by describing each dihedral angle ($\alpha$, $\beta$, $\gamma$, . . .) as either $g^+$ ($0° < \phi < 120°$), $g^-$ ($0° > \phi > -120°$), or a ($120° < \phi < 240°$). The 200-kcal/mol energy cutoff may seem overly generous, but preliminary studies clearly showed that structures with energies this high could, upon complete optimization, attain energies comparable to those of the most stable conformers.

The magnitude of the problem thus became clear, especially when one considers a presumably more flexible structure such as C16, for which the number of feasible conformers would likely be astronomical. We therefore repeated the above procedure for C12 with a closure criterion of 2.5 Å. This led to a total of 838 unique C12 structures with initial energies less than 200 kcal/mol. We then optimized the geometries of all of these structures using the NOH field, a Newton–Raphson optimization algorithm, and a convergence criterion of 0.1 kcal/mol. The naphthalene was frozen at the standard geometry.[29] This resulted in 778 unique minima. The steric energies of these minima relative to the lowest energy structure, $E_{rel}$, ranged from 0 to 47 kcal/mol, but the vast majority (626) were less than 14 kcal/mol above the "ground state". It must be emphasized that the NOH field with a 0.1-kcal/mol convergence criterion is a relatively crude level of optimization. We wished to evaluate how many such structures could feasibly be populated significantly at room temperature or could lie along the enantiomerization pathway. Thus, one must be generous when considering the range of energies for acceptable structures. Two views of a typical C12 minimum energy structure are given in Figure 8.

We have analyzed these C12 structures in some detail. One feature we wished to ascertain was whether there were conformational restrictions on the chain. One might have anticipated that the early parts of the chain would be somewhat restricted so that the chain could get out away from the naphthalene and then aim in the general direction of the other oxygen. Table IV shows the results of our search for conformational preferences in the 778 C12 minima described above. Apart from a clear avoidance of the anti conformation by the $\beta$ angle, there are no strong preferences along the chain. Clearly, the presence of the naphthalene ring does not significantly restrict the available conformations of the chain.

With steric energies in hand for fully optimized structures, we were able to test our assumption that these naphthalenophanes are essentially strain free in the ground state. This could be done by evaluating $\Delta H°$ for the homodesmotic reaction[30] in which

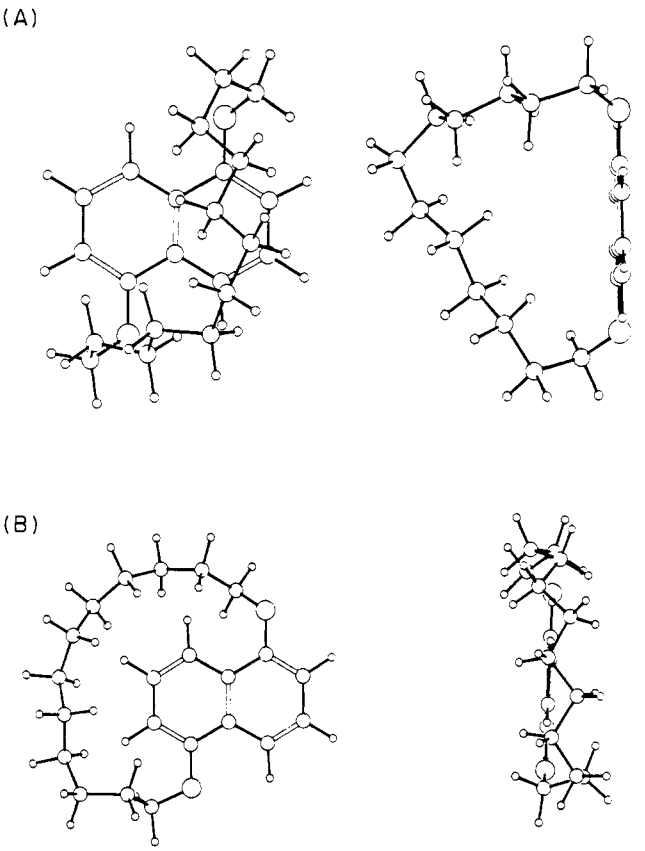


**Figure 8.** (a) Two views of a low-lying, ground-state conformation for C12. (b) Two views of a low-lying "transition-state" structure for C12.

1,5-dimethoxynaphthalene plus the linear alkane with $(n + 2)$ carbons were converted to **1** plus two ethanes. In order to get a more meaningful estimation of this quantity, we wished to use the more reliable MM2 force field. Thus, the five lowest energy NOH structures for each of C12 and C14–C16 (see below) were fully optimized using MM2. The lowest energy of these structures was then used for strain evaluations. In this manner, C12 was calculated to have a strain energy of only 7.5 kcal/mol. The strain energies of C14, C15, and C16 were all in the range 3–7 kcal/mol. Thus, the assumption that these structures are essentially strain free was confirmed.

All the NMR data suggested real or time-averaged $C_2$ symmetry for C14–C16. Time-averaged symmetry seemed to be the much more likely explanation of the spectra, and, indeed, almost all the low-energy structures calculated are asymmetric. In order to confirm the viability of the notion that these many asymmetric conformers can interconvert rapidly to produce a time-averaged $C_2$ structure, we have performed several, standard angle-driving calculations[11] using the complete MM2 field. These calculations indicate that the barriers are quite small (<4 kcal/mol), and that the rotations along the chain are not neccesarily coupled. For example, one can drive one angle along the chain from gauche (+) to anti, and the rest of the chain will readjust, but there will be no other changes in the conformational descriptor of the chain.

The important conclusion that emerges from all of the above studies on the ground state of C12 is that, despite the presence of the naphthalene system, the aliphatic chains of the naphthalenophanes studied have essentially the properties of an unrestricted, polymethylene chain. That is, the molecules are nearly strain free and possess a very large number of low-energy conformers, and these conformers can interconvert readily over small barriers. We emphasize again that these conclusions result primarily from our studies on C12, and carry over with even greater force to C14–C16.

(30) George, P.; Trachtman, M.; Bock, C. W.; Brett, A. M. *Tetrahedron* **1976**, *32*, 317–323.

**Table V.** Results of Structure Generation and Minimization

| structure | ground states | | transition states | |
|---|---|---|---|---|
| | guesses[a] | minima | guesses[c] | transition states |
| C12 | 26 | 26 | 44 | 6 |
| C14 | 326 | 326 | 266 | 35 |
| C15 | 592 | 590 | 594 | 77 |
| C16 | 2619 | | 1738 | 327 |
| C16 | 810[b] | 805 | | |

[a] Closure criterion = 1.0 Å; energy cutoff = 200 kcal/mol. [b] Energy cutoff = 100 kcal/mol. [c] Closure criterion = 2.0 Å; energy cutoff = 500 kcal/mol.

The preliminary studies on C12 indicated that a complete enumeration of all possible conformers for C14–C16 would be infeasible. We therefore adopted the following approach. Rather than attempt to quantitatively reproduce the $\Delta H^{\ddagger}$ and $\Delta S^{\ddagger}$ values of Table III, we sought to rationalize the trends in the data. More specifically, we hoped to gain some insight into the remarkable change in $\Delta S^{\ddagger}$ on going from C14 and C15 to C16. In such a study, the crucial consideration is to apply a *consistent level of theory* to all structures calculated. In this way, the trends in experimental data can be analyzed, even though precise quantitative agreement is not obtained.

There are, in principle, two effects that contribute to $\Delta S^{\ddagger}$ for reactions such as the enantiomerizations of C14–C16. The first is due to the difference in entropy content of the ground and transition states. This is merely the entropy difference between two conformers of the same molecule and will be dominated by differences in the partition function associated with internal degrees of freedom, that is, the vibrational and rotational modes. We shall refer to this as the intrinsic entropy of activation, $\Delta S^{\ddagger}_{int}$. As discussed below, for the present process there are many "ground states", and most likely many transition states. This will lead to a large number of reaction paths, each with its own $\Delta S^{\ddagger}_{int}$.

The second contributor to $\Delta S^{\ddagger}$ is a statistical term, $\Delta S^{\ddagger}_{stat}$. This arises from the fact that there is not just one ground-state conformation and one transition state, but rather there are large numbers of both. If, as a first approximation, we consider all the low-lying "ground-state" conformers we have found to be degenerate and likewise for the "transition states", then $\Delta S^{\ddagger}_{stat}$ is as in eq 1, in which $g_1$ is the degeneracy of the ground state and $g_2$ the degeneracy of the transition state.

$$\Delta S^{\ddagger}_{stat} = R \ln g_2/g_1 \quad (1)$$

It is useful to first consider the values $g_1$ and $g_2$ must have if $\Delta S^{\ddagger}_{stat}$ is the major contributor to $\Delta S^{\ddagger}$. For example, a $\Delta S^{\ddagger}$ of −20 eu would require $g_1/g_2 = 24\,000$. More significantly, if the 20-eu *difference* in $\Delta S^{\ddagger}$ values between C15 and C16 is due entirely to $\Delta S^{\ddagger}_{stat}$, then the ratio of the $g_1/g_2$ ratios for C16 and C15 would have to be 24 000. Thus, one of our primary goals has been to search for a dramatic change in the statistics of ground-state vs. transition-state conformations for C14 and C15 vs. C16. Only a very substantial change could make a sizable contribution to $\Delta S^{\ddagger}$.

The first step was to analyze C14–C16 in a manner similar to the above treatment of C12. Table V summarizes the structure-generation results for these molecules. In order to keep the problem manageable, a more severe closure criterion (1.0 Å) was adopted. As expected, the longer the chain the greater the number of viable structures that was generated (Table V). At this level only 26 structures were generated for C12. While a substantially larger number of structures was generated for C16 than for C15 or C14, the difference was less than a factor of 5. This would seem to be a first indication that $\Delta S^{\ddagger}_{stat}$ is not the major reason for the $\Delta\Delta S^{\ddagger}$ between C15 and C16.

Table V also shows the number of minima obtained from these input guesses. Unfortunately, all 2619 C16 structures could not be optimized, and so only the 810 structures with initial energies less than 100 kcal/mol ($E_0$ = 60 kcal/mol) were optimized. As with C12 most input structures led to unique minima.

Since $\Delta S^{\ddagger}_{stat}$ depends not only on the number of ground-state structures, but also on the number of transition states (eq 1), we wished to determine whether there was a dramatic difference between C14/C15 and C16 in this respect. We therefore needed a way to evaluate relative transition-state degeneracy for the three structures. This was accomplished through a modification of the structure-generation program.

**Table VI.** Distribution of Ground and "Transition" States from Table V as a Function of Energy[a]

| $E_{rel}$ | C14 | | C15 | | C16 | |
|---|---|---|---|---|---|---|
| | GS | TS | GS | TS | GS[b] | TS |
| 0–2 | 5 | 0 | 3 | 0 | 5 | 0 |
| 2–4 | 10 | 0 | 5 | 0 | 22 | 2 |
| 4–6 | 34 | 0 | 21 | 2 | 63 | 1 |
| 6–8 | 37 | 0 | 54 | 2 | 125 | 13 |
| 8–10 | 61 | 1 | 83 | 4 | 203 | 16 |
| 10–12 | 53 | 3 | 114 | 2 | 181 | 30 |
| 12–14 | 53 | 1 | 101 | 12 | 127 | 35 |
| 14–16 | 35 | 7 | 93 | 12 | 56 | 36 |

[a] Energies in kcal/mol. GS = ground state; TS = transition state. [b] Only the 810 structures below the 100-kcal/mol energy cutoff were optimized.

We first assumed that transition-state structures would in general have the aliphatic chain roughly in the plane of the naphthalene. That is, the chain would be looping around the edge of the ring system, rather than across one face. Thus, with the naphthalene ring fixed in the $xy$ plane, we forced all carbons of the chain to have an absolute value of <2.0 Å for their $z$ coordinates. Additionally, instead of treating the steric exclusion volume of the naphthalene as an ellipsoid, it was treated as an infinitely tall box, thereby preventing passage of the chain over the naphthalene. Structures were then generated in the usual manner and subjected to the closure optimization procedure as above, except that the closure criterion was opened up to 2.0 Å, and the initial energy cutoff was expanded to 500 kcal/mol. These structures were then optimized (NOH, 0.1 kcal/mol convergence) and, based on the following criterion, transition-state representatives were chosen from the resulting minima. With the naphthalene still in the $xy$ plane, the $z$ coordinates of the chain carbons were averaged, and this average was required to be <0.25 Å. Note that positive $z$ values will cancel with negative $z$ values in the summation, thereby producing a small average $z$. Additionally, structures with at least four carbons on each side of the ring were retained. Both these criteria were intended to limit the list of transition state structures to only those conformations in which the chain really does wrap around the edge of the naphthalene. The actual numerical criteria are somewhat arbitrary, but the important point is that they were applied consistently throughout the series. It must be remembered that the structures so obtained are not transition states. In fact, they are true minima. However, the energetics and statistics of such structures can provide a useful, qualitative model for the actual transition states. Two views of a typical "transition state" structure for C12 are given in Figure 8.

The results of this study are summarized in Tables V and VI. A fairly large number of guess structures were generated, but upon optimization (NOH field), a large number of conformers optimized to give structures that failed to meet the various transition-state criteria. Still, significant numbers of transition-state structures were obtained. As expected, the longer the chain, the greater the number of transition states (Table V). Concerning the above statistical arguments, the substantial increase in the number of viable ground-state conformations for C16 relative to C14–C15 is paralleled by an increase in transition-state structures. This holds true whether one considers the total number of structures (Table V) or only the relatively low-lying ones (Table VI). Thus, $g_1/g_2$ for C16 should not be dramatically different from that for C14–C15. We therefore conclude that $\Delta S^{\ddagger}_{stat}$ is *not* the dominant contributor to the $\Delta S^{\ddagger}$ values observed.

What is clear from Table VI is that there are many more low-lying transition states for C16 than for C14–C15. While not significant in a statistical sense, this does imply that, within the constraints of the enantiomerization transition state, C16 expe-

riences much more conformational freedom than C14 or C15. Thus, the overall implications of these studies are that C14–C16 are all quite unrestricted in the ground state, but only C16 retains this freedom in the enantiomerization transition state. We believe this is the most important factor in differentiating $\Delta S^{\ddagger}$ for C14 and C15 vs. C16.

## Conclusions

The cyclophanes C14, C15, and C16 represent good models for unrestricted polymethylene chains and macrocyclic compounds in their ground conformational states. However, much of the conformational freedom in C14 and C15 is lost in the enantiomerization transition states, as reflected by the remarkably large, negative $\Delta S^{\ddagger}$ values for the enantiomerization reactions. Presumably, this is becuase the chains must adopt a relatively constrained, "extended" conformation in order to get around the naphthalene frame. The magnitude of the effect is quite substantial, representing a rate retardation at room temperature of a factor of $10^5$ for C14. A similar diminution in binding efficiency would occur for a structure with comparable structural features that is similarly unconfined in the unbound state, but considerably constrained by binding.

The most remarkable finding of the present work is the complete disappearance of the entropy effect on going to C16. Note that an analysis based solely on $\Delta G^{\ddagger}$ (Table III) would give the false impression that the series C14, C15, C16 is well behaved and follows the obvious trend that greater chain length gives a smaller barrier. Our MM results suggest that this effect arises because the C16 chain is simply long enough to achieve enantiomerization transition states that are still conformationally quite flexible. From the data in Table III, it would appear that such conformations are achieved at the expense of a slightly higher $\Delta H^{\ddagger}$, relative to C15. Clearly, these results emphasize the dangers of extrapolating activation parameters among even very closely related compounds. From a more practical standpoint, the present results demonstrate that the ring sizes of C14 and C15 are the most appropriate for studies of substituent and solvent effects, and such further studies are underway.

## Experimental Section

Routine NMR spectra were recorded on a Varian EM-390 spectrometer or a JEOL FX-90Q spectrometer. High-field NMR were recorded on a Varian XL-200 or a Bruker WM-500 spectrometer. Mass spectra and elemental analyses were obtained at the Caltech Analytical Facility. Melting points were determined on a Thomas-Hoover Uni-Melt and are corrected.

**[2,2,4,4-$^2H_4$]Glutaric Acid.**[31] Glutaric acid (20 g, 0.15 mol) and sodium hydroxide (13 g, 0.33 mol) were dissolved in 35 mL of $D_2O$ (99.8% $^2H$) and the mixture was placed in a stainless steel autoclave and heated to 150 °C. After 24 h, the mixture was cooled, the bomb as opened, and the water was completely removed at 50 °C under vacuum. Another 35 mL of $D_2O$ and 1.22 g of NaOH were added to the residue, and another exchange was performed at 150 °C. After a total of five such exchanges, the reaction mixture was acidified with concentrated HCl and then continuously extracted overnight with diethyl ether. Removal of the ether gave 14 g (70%) of glutaric acid as white crystals. $^1H$ NMR inicated 99.8% deuterium incorporation.

**[2,2,5,5-$^2H_4$]Adipic acid** was prepared exactly as above for glutaric-$d_4$ acid. After five exchanges, $^1H$ NMR indicated 99.8% deuterium incorporation.

**General Conversion of Diacids to Dibromides.** Standard procedures were used. The diacid was reduced with $BH_3$·THF to the diol using the method of Brown.[32] When $^2H$ incorporation was required, $BD_3$ was prepared from $NaBD_4$ and $BF_3$·etherate, according to Brown.[33] By NMR, the $^2H$ incorporation at these positions was estimated to be 96.0%. The diols were converted to dibromides using an $HBr/H_2SO_4$ mixture according to the method of Kamm and Marvel.[34]

**General Grignard Coupling of Dibromides.** The procedure used was an adaptation of the method of Friedman and Shani,[35] and all the dibromides are previously reported compounds. Thus, to a THF solution of the preformed di-Grignard reagent from the appropriate dibromide (see Scheme II) were added $Li_2CuCl_4$ and a twofold excess of the second dibromide in THF. The mixture was stirred at room temperature for 8 h, quenched with 2 N HCl, and extracted with $CH_2Cl_2$. The organic layer was dried ($Na_2SO_4$) and rotary evaporated and the product was isolated by vacuum distillation.

**General Procedure for Cyclophane Synthesis.** The procedures of Mandolin et al.[12a] were followed exactly. Thus, the appropriate dibromide (see Scheme I) and a fivefold excess of 1,5-dihydroxynaphthalene were treated with KOH in ethanol at reflux for 3–5 h. The solvent was removed; the solid residue was finely ground and then extracted with *n*-hexane for 2 days using a Soxhlet apparatus. The resulting product was further purified by flash chromatography on silica gel (ether/petroleum ether, 1:4), to give **2**: mp (% yield) for $n$ = 14, 77–78 °C (31%); $n$ = 15, 79–81 °C (41%); $n$ = 16, 81–82 °C (27%).

These bromides (**2**) were then subjected to the standard ring-closure procedure.[12a] Thus, separate $Me_2SO$ solutions of **2** and of tetramethylammonium hydroxide were added via two syringe pumps to a small amount of $Me_2SO$ at 80 °C over a 2-h period. Standard workup and flash chromatography on silica gel (benzene/petroleum ether, 1:5) gave the cyclophanes, in yields of 33, 64, and 63% for C14, C15, and C16, respectively. Proton NMR are shown in Figure 1.

**C14**: mp 71–72 °C; $^{13}C$ NMR ($CDCl_3$) 153.83, 127.44, 124.71, 114.18, 106.38, 67.26, 29.31, 28.21, 26.97, 26.71, 24.18; MS (rel intensity) 355 (20), 354 (78), 161 (18), 160 (100), 131 (15). Calcd for $C_{24}H_{34}O_2$: 354.2559. Found: 354.2550.

**C15**: mp 68–69 °C; $^{13}C$ NMR ($CDCl_3$) 154.15, 127.44, 124.78, 114.31, 106.25, 67.33, 28.25, 28.40, 29.26, 27.62, 26.97, 24.63; MS (rel intensity) 369 (19), 368 (67), 161 (13), 160 (100), 131 (11). Anal. Calcd for $C_{25}H_{36}O_2$: C, H.

**C16**: mp 108–109 °C; $^{13}C$ NMR ($CDCl_3$) 154.28, 127.12, 124.78, 114.12, 105.54, 66.61, 29.70, 28.79, 27.95, 27.75, 26.06, 23.79; MS (rel intensity) 383 (15), 382 (47), 161 (18), 160 (100), 131 (25). Calcd for $C_{26}H_{38}O_2$: 382.2872. Found: 382.2893.

**DNMR Studies.** All DNMR studies involved the $\gamma$ protons of the labeled cyclopanes derived from dibromides **6**, **7**, and **8**. All studies were conducted at 500.13 MHz on the Bruker WM-500, with the exception of the C14 line-shape study, which was performed at 200 MHz on the Varian XL-200. The temperature controllers on both probes were frequently calibrated using MeOH (low temperature) or ethylene glycol (high temperature) and the standard van Geet relationship.[36] The solvents used were nitrobenzene-$d_5$ (C14-CLS), *o*-dichlorobenzene-$d_4$ (C14-SST), $CD_2Cl_2$ (C15), and $CF_2Cl_2/CD_2Cl_2$, 19:1 by volume (C16). Line-shape analyses were performed using the program DNMR3.[37]

**Acknowledgment.** We gratefully acknowledge the 3M Corporation for partial support of this work through a Young Faculty Grant. This work made use of the NSF Southern California Regional NMR Facility (NSF Grant 79-16324) and the Dreyfus-NSF Chemistry Computing Center.

**Registry No. 2** ($n$ = 14), 94427-65-3; **2** ($n$ = 15), 94427-66-4; **2** ($n$ = 16), 94427-67-5; **3**, 14130-72-4; **4**, 94427-58-4; **5**, 94427-59-5; **6**, 94427-60-8; **6** (cyclophane), 94427-63-1; **7**, 94427-61-9; **7** (cyclophane), 85851-50-9; **8**, 94427-62-0; **8** (cyclophane), 94427-64-2; **C14**, 94427-68-6; **C15**, 85851-49-6; **C16**, 94427-69-7; [2,2,4,4-$^2H_4$]glutaric acid, 19136-99-3; [2,2,5,5-$^2H_4$]adipic acid, 19031-55-1; glutaric acid, 110-94-1; adipic acid, 124-04-9; 1,4-dibromobutane, 110-52-1; 1,5-naphthalenediol, 83-56-7.

(31) Atkinson, J. G.; Csakvary, J. J.; Herbert, G. T.; Stuart, R. S. *J. Am. Chem. Soc.* **1968**, *90*, 498–499.
(32) Yoon, N. M.; Pak, C. S.; Brown, H. C.; Krishnamurthy, S.; Stocky, T. P. *J. Org. Chem.* **1973**, *38*, 2786–2792.
(33) Brown, H. C.; Sharp, R. L. *J. Am. Chem. Soc.* **1968**, *90*, 2915–2927.
(34) Kamm, O.; Marvel, C. S. "Organic Synthesis"; Wiley: New York, 1941; Collect. Vol. I, pp 25–41.
(35) Friedman, L.; Shani, A. *J. Am. Chem. Soc.* **1974**, *96*, 7101–7103.
(36) Van Geet, A. L. *Anal. Chem.* **1970**, *42*, 679–680. Van Geet, A. L. *Ibid.* **1968**, *40*, 2227–2229.
(37) Kleier, D. A.; Binsch, G. *QCPE* **1979**, *11*, 165.